Condition monitoring of the front axle of a load haul dumper with real order derivatives and generalised norms

[1] Juhani Nissilä, [2] Sulo Lahdelma and [1] Jouni Laurila

[1] Mechatronics and Machine Diagnostics Research Group, Faculty of Technology
P.O. Box 4200, FI-90014 University of Oulu, Finland
E-mail: juhani.nissila@oulu.fi, jouni.laurila@oulu.fi

[2] Engineering Office Mitsol Oy
Tirriäisentie 11, FI-90540 Oulu, Finland
E-mail: sulo.lahdelma@mitsol.inet.fi

Abstract

Fractional calculus and generalised norms provide a powerful toolkit for analysing vibration from rotating machines. They have been used effectively in the condition monitoring of immobile machines. A harsh environment and varying operating conditions complicate the reliable condition monitoring of mobile machines in underground mining industry. In this paper, we focus on the condition monitoring of the front axle of a load haul dumper and the numerical calculation of complex order derivatives and integrals. Measurements are performed with accelerometers, which measure horizontal and vertical vibrations near the planetary gearboxes. A tachometer records the rotational speed of the drive shaft, which is essential for recognising different operation stages of the machine. We describe how the mentioned difficulties can be overcome and what real order derivatives and generalised norms can reveal about the condition of the axle. An improved algorithm for the numerical calculation of complex order derivatives and integrals is given.

Keywords: load haul dumper, LHD, axle, planetary gearbox, condition monitoring, diagnostics, real and fractional order derivatives, l_p norms, *MIT* indices

1. Introduction

This paper provides a detailed discussion of the numerical calculation of real and complex order derivatives and integrals using the discrete Fourier transform. The improved algorithm is utilised to analyse vibration measurements from the front axle of a load haul dumper (LHD). These machines operate in harsh conditions where failures may be difficult to repair. The machine under study is a Sandvik LH 261 working underground in the Pyhäsalmi mine. Four accelerometers were mounted on its front axle housing. They measure horizontal and vertical vibrations near the planetary gearboxes on either side. A tachometer records the rotational speed of the drive shaft. The measurements included in this study cover a period of 271 days and more data are still being collected. Signals that were recorded when the LHD was moving at constant speed and without a load

proved to be useful for monitoring condition. The generalised norms are calculated using different orders of derivatives $\alpha \in \mathbb{R}$ and norms $p \in \mathbb{R}$. These are divided by reference values when the machine is in good condition in order to form a three dimensional surface to reveal which of the norms have changed the most. Trend analysis of different norms is performed for the whole measurement period.

2. Real and complex order derivatives and integrals

2.1 Definitions

Functions of the form

$$x(t) = Xe^{i\omega t}, \tag{1}$$

where X and ω are constants and $i = \sqrt{-1}$ can be differentiated n times and we obtain the expression

$$x^{(n)}(t) = (i\omega)^n Xe^{i\omega t}. \tag{2}$$

In references [1,2,3,4] Lahdelma et al. have defined real order derivatives and integrals of function (1) by replacing $n \in \mathbb{N}$ with a real number $\alpha \in \mathbb{R}$

$$x^{(\alpha)}(t) = (i\omega)^\alpha Xe^{i\omega t}, \tag{3}$$

where $(i\omega)^\alpha = |\omega|^\alpha \big(i \cdot \mathrm{sign}(\omega)\big)^\alpha = |\omega|^\alpha e^{i\alpha\frac{\pi}{2}\mathrm{sign}(\omega)}$. The function sign is the signum function that extracts the sign of a real number. Equation (3) is further generalised to derivatives and integrals of complex order $z = \alpha + i\beta$ where $\alpha, \beta \in \mathbb{R}$ [5,6]

$$x^{(z)}(t) = (i\omega)^z Xe^{i\omega t}, \tag{4}$$

and only the principal value of the function $(i\omega)^z$ is considered, which gives us $(i\omega)^z = e^{z\ln(|\omega|)+iz\frac{\pi}{2}\mathrm{sign}(\omega)}$. In the case of vibration signals the constant X represents the amplitude at the angular frequency $\omega = 2\pi\nu$ in the signal's spectrum. This can be stated mathematically with the *Fourier transform* $X(\nu)$ of the signal $x(t)$

$$\mathcal{F}\{x(t)\} = X(\nu) = \int_{-\infty}^{\infty} x(t)e^{-i2\pi\nu t}\,\mathrm{d}t. \tag{5}$$

Its *inverse transform* is defined as

$$\mathcal{F}^{-1}\{X(\nu)\} = \int_{-\infty}^{\infty} X(\nu)e^{i2\pi\nu t}\,\mathrm{d}\nu. \tag{6}$$

In suitable function spaces the inverse transform returns the original signal. If this is the case, then the original function can be written as a double integral, which is called the *Fourier integral theorem.*

Fourier derived in 1822 in his book *Théorie analytique de la chaleur* [7] a form of integral theorem (here shown with modern notation)

$$x(t) = \frac{1}{2\pi}\int_{-\infty}^{\infty} x(\nu)\int_{-\infty}^{\infty} \cos(pt - p\nu)\,\mathrm{d}p\,\mathrm{d}\nu, \tag{7}$$

and used it to present the real order derivatives and integrals of function x in the form

$$\frac{\mathrm{d}^\alpha}{\mathrm{d}t^\alpha}x(t) = \frac{1}{2\pi}\int_{-\infty}^{\infty} x(\nu)\int_{-\infty}^{\infty} p^\alpha \cos\left(pt - p\nu + \alpha\frac{\pi}{2}\right)\,\mathrm{d}p\,\mathrm{d}\nu. \tag{8}$$

We define differintegrals $x^{(z)}$ for such functions x whose Fourier transforms X and inverse transforms of $(i2\pi\nu)^z X$ exist. Let $z \in \mathbb{C}$ and X is the Fourier transform of x. The *differintegral* of order z is

$$\begin{aligned} x^{(z)}(t) &= \mathcal{F}^{-1}\big\{(i2\pi\nu)^z X(\nu)\big\} \\ &= \int_{-\infty}^{\infty} (i2\pi\nu)^z X(\nu)\, e^{i2\pi\nu t}\,\mathrm{d}\nu, \end{aligned} \tag{9}$$

where $(i2\pi\nu)^z = e^{z\ln(2\pi|\nu|)+iz\frac{\pi}{2}\mathrm{sign}(\nu)}$.

In many textbooks on fractional calculus this is not presented as a definition of a differintegral, but rather as a way of representing (and calculating) differintegrals based on other definitions. Similar definitions are also used in [8,9], for example. For $\mathrm{Re}(z) < 0$ it is convenient to assume that the signal has zero mean value, i.e. $\int_{-\infty}^{\infty} x(t)\,\mathrm{d}t = X(0) = 0$, or otherwise the zero frequency component would be amplified into a Dirac delta function. A closely related definition was considered by Hermann Weyl in 1917 [10] using Fourier series.

The usefulness of definition (9) in vibration mechanics and other physical applications is that the object may vibrate with any angular frequency $\omega = 2\pi\nu \in \mathbb{R}$ and the effect of these frequencies on fractional derivatives and integrals is plainly seen. Even more importantly it does not include a built-in ansatz, as most of the definitions of fractional calculus in the time domain do [11]. For vibration signals this means that with the Fourier definition one takes into account the whole past history of the vibration and does not assume that it was zero at some exact time in the past. In the article [1] Lahdelma has studied the transition of the real order derivatives and integrals $(i\omega)^\alpha X e^{i\omega t}$ in the complex plane as the order of differentiation and integration changes.

In practice, signals are sampled with sample time Δt and the length of the signal is finite. Then we have a sampled sequence $x_0, \ldots, x_{N-1}$ and we can approximate the signal's Fourier transform with the *Discrete Fourier transform* (DFT)

$$\mathcal{F}\{x_n\} = X_k = \frac{1}{N}\sum_{n=0}^{N-1} x_n e^{-i2\pi kn/N}. \tag{10}$$

Its *inverse transform* (IDFT) is

$$\mathcal{F}^{-1}\{X_k\} = x_n = \sum_{k=0}^{N-1} X_k e^{i2\pi kn/N}. \tag{11}$$

Discrete Fourier transform and its inverse are complex-valued sequences of equal length. They are also N-periodic and the inverse returns the original sequence. DFT is therefore a discrete approximation of the signals spectrum but also contains all the information needed to return the original sequence.

The problem with the DFT and IDFT is that they assume the signal to be periodic. This can be improved by multiplying the signal with a suitable window function. When calculating real order derivatives and integrals it is desirable that the signal is distorted in the time domain as little as possible. Therefore, the window function should have quite rapid ascent and descent.

A simple window function is constructed from the Hann window by using it in the ascent and descent parts of the window

$$w_1(t) = \begin{cases} 0, & \text{if } t \leq 0 \\ 0.5\left(1 - \cos\left(\pi \frac{t}{T/\epsilon}\right)\right), & \text{if } 0 < t < T/\epsilon \\ 1, & \text{if } T/\epsilon \leq t \leq T/2 \\ w_1(T-t), & \text{if } t > T/2, \end{cases} \tag{12}$$

where ϵ is the portion of T for ascent and descent. In the books [12,13] examples are given of $\epsilon = 10$.

Lahdelma and Kotila introduced in the article [6] a window function

$$w_2(t) = \begin{cases} 0, & \text{if } t \leq 0 \\ \left(\int_0^{T/\epsilon} e^{\left(\tau(\tau - T/\epsilon)\right)^{-1}} \mathrm{d}\tau\right)^{-1} \int_0^t e^{\left(\tau(\tau - T/\epsilon)\right)^{-1}} \mathrm{d}\tau, & \text{if } 0 < t < T/\epsilon \\ 1, & \text{if } T/\epsilon \leq t \leq T/2 \\ w_2(T-t), & \text{if } t > T/2, \end{cases} \tag{13}$$

and used the value $\epsilon = 8$ in their calculations. It can easily be seen that all the derivatives of w_2 are continuous and, therefore, it preserves the continuity properties of the original signal.

2.2 Numerical algorithm

For discrete samples one cannot straightforwardly calculate differintegrals according to definition (9). However, one can form the discrete components X_k of DFT. Then the IDFT formula (11) defines a trigonometric interpolation of the function that can be differintegrated in the frequency domain by multiplying the DFT components X_k with $(i2\pi k/T)^z$ and taking IDFT of this new sequence. The numbers k are problematic, because due to the N-periodicity of IDFT the interpolant gets the same values at discrete points even if k was replaced with $k + m_k N$, where $m_k \in \mathbb{Z}$. Bigger k (higher frequency) creates more oscillation between the sample points, which has a major impact on the differintegrals. If we want the interpolant to be as smooth as possible, the best choices should be from the interval $-N/2 \leq k \leq N/2$. In the reference [14] this differentiation of the triconometric interpolant has been studied with respect to the 1st and 2nd derivatives of the function. In this article the order of differintegration is allowed to be $z \in \mathbb{C}$ for the sake of completeness, although only real order differintegrals are utilised in the experimental part. Trigonometric interpolation is a function of the continuous time variable t

$$x(t) = \sum_{k=0}^{N-1} X_k e^{i2\pi(k + m_k N)t/T},$$

which at the sample points t_n receives the values x_n for all $m_k \in \mathbb{Z}$, where $t_n = \Delta t \cdot n$, $n = 0, 1, \ldots, N\text{-}1$ and $T = \Delta t \cdot N$. We want the interpolation to oscillate as little as possible between the sample points. In the reference [14] $\frac{1}{T}\int_0^T |x'(t)|^2 \,\mathrm{d}t$ was minimised, but it was also mentioned, that the same result can be obtained by limiting the frequencies

$$|k + m_k N| \leq \frac{N}{2}. \tag{14}$$

When $0 \leq k < N/2$, equation (14) implies $m_k = 0$ and when $0 \leq k < N/2$, we get $m_k = -1$. Therefore we get the values $-N/2 < k < N/2$. The problem is solved if N is odd. However if N is even, the term $N/2$ is problematic. Frequency limitation (14) gives $m_k = 0$ or $m_k = -1$. Let's divide it between both of these frequencies

$$\begin{aligned} &X_{N/2}\left[u e^{i2\pi\frac{N}{2}t/T} + (1-u)e^{i2\pi(\frac{N}{2}-N)t/T}\right] \\ &= X_{N/2}\left[u e^{i\pi Nt/T} + (1-u)e^{-i\pi Nt/T}\right], \end{aligned}$$

where u could be any complex number, since at the sample points $t_n = \Delta t \cdot n = \frac{T}{N}n$ we have $e^{\pm i\pi n} = (-1)^n$ and the right IDFT component is regained

$$X_{N/2}(-1)^n\left[u + (1-u)\right] = X_{N/2}(-1)^n.$$

In the reference [14] the number u was decided by minimising $\frac{1}{T}\int_0^T |x'(t)|^2 \,\mathrm{d}t$ but a simpler way is to demand that an interpolant of a real-valued signal must be real-valued everywhere. For real-valued signals the DFT values have the symmetry $X_k = \overline{X_{N-k}}$ and therefore X_0 and $X_{N/2}$ are real-valued. These symmetric terms form in pairs cosine and sine terms. Therefore, the multiplier of the lone $X_{N/2}$ must be real, which is true if $u = 1/2$

$$X_{N/2}\frac{1}{2}\left[e^{i\pi Nt/T} + e^{-i\pi Nt/T}\right] = X_{N/2}\cos\left(\frac{\pi Nt}{T}\right).$$

We finally have the *trigonometric interpolation of minimal oscillation* [14]

$$\begin{aligned} x(t) &= X_0 + \sum_{0<k<N/2}\left(X_k e^{i2\pi kt/T} + X_{N-k}e^{-i2\pi kt/T}\right) + X_{N/2}\cos\left(\frac{\pi Nt}{T}\right) \\ &= \sum_{0\leq k<N/2} X_k e^{i2\pi kt/T} + \sum_{-N/2<k<0} X_{N+k}e^{i2\pi kt/T} + X_{N/2}\cos\left(\frac{\pi Nt}{T}\right). \end{aligned} \tag{15}$$

Let us differintegrate interpolation (15) $z \in \mathbb{C}$ times with the definition (9)

$$\begin{aligned} x^{(z)}(t) = &\sum_{0\leq k<N/2}\left(\frac{2\pi ki}{T}\right)^z X_k e^{i2\pi kt/T} + \sum_{-N/2<k<0}\left(\frac{2\pi ki}{T}\right)^z X_{N+k}e^{i2\pi kt/T} \\ &+ \left(\frac{\pi N}{T}\right)^z X_{N/2}\cos\left(\frac{\pi Nt}{T} + z\frac{\pi}{2}\right), \end{aligned}$$

and compute it at the sample points $t_n = \frac{T}{N}n$

$$\begin{aligned} x_n^{(z)} = &\sum_{0\leq k<N/2}\left(\frac{2\pi ki}{T}\right)^z X_k e^{i2\pi kn/N} + \sum_{-N/2<k<0}\left(\frac{2\pi ki}{T}\right)^z X_{N+k}e^{i2\pi kn/N} \\ &+ \left(\frac{\pi N}{T}\right)^z X_{N/2}\cos\left(\pi n + z\frac{\pi}{2}\right). \end{aligned}$$

The last term has to be written in the form

$$\begin{aligned}
&\left(\frac{\pi N}{T}\right)^z X_{N/2}\,\frac{1}{2}\left(e^{i\pi n+iz\frac{\pi}{2}}+e^{-i\pi n-iz\frac{\pi}{2}}\right)\\
&=\left(\frac{\pi N}{T}\right)^z \frac{1}{2}\left(i^z+(-i)^z\right)X_{N/2}(-1)^n\\
&=\left(\frac{\pi N}{T}\right)^z \cos\left(z\frac{\pi}{2}\right)X_{N/2}(-1)^n
\end{aligned}$$

to get the expression in the form of IDFT. Apart from this last term all the values X_k get multipliers $(2\pi ki/T)^z$, $-N/2 < k < N/2$ and for $X_{N/2}$ we get the multiplier

$$\left(\frac{\pi N}{T}\right)^z \cos\left(z\frac{\pi}{2}\right). \tag{16}$$

This multiplier is zero only at the zeroes of the cosine function at $z = 2n-1, n \in \mathbb{N}$.

Previous calculations were performed because of a single problematic term in the DFT. If N is odd, none of those calculations matter. However, to utilise the speed of the FFT algorithm we need even N [(15)].

Algorithm 1. Differintegration in frequency space

1. Calculate the DFT X_k, $0 \le k \le N$-1 of the sequence x_n, $0 \le n \le N$-1 with the FFT algorithm
$$X_k = \mathcal{F}\{x_n\}.$$
2. Calculate a new sequence G_k, $0 \le k \le N$-1 and $G_0 = 0$
$$\begin{aligned}
G_k &= \left(\frac{2\pi ki}{T}\right)^z X_k, \qquad 0 < k < N/2\\
G_{N+k} &= \left(\frac{2\pi ki}{T}\right)^z X_{N+k}, \quad -N/2 < k < 0\\
G_{N/2} &= \left(\frac{\pi N}{T}\right)^z \cos\left(z\frac{\pi}{2}\right)X_{N/2} \quad \text{(if } N \text{ is even)}.
\end{aligned}$$
3. Calculate the differintegrated sequence $x_n^{(z)}$ with the IFFT
$$x_n^{(z)} = \mathcal{F}^{-1}\{G_k\}.$$

To provide a simple example of the usefulness of the window functions and the effectiveness of the Algorithm 1, we differentiate the function $\cos(\pi t)$ at the interval $[0, 7]$. The periodic continuation of this function is not continuous, since $\cos(0) = 1 \neq -1 = \cos(7\pi)$. Figure 1 shows the convergence of the absolute error of the first derivative at the point

$t = 3.5$ as the number of sample points increase. Values of the window function w_2 (13) have been integrated numerically with the trapezoidal rule and the Simpson's rule, but these two perform almost identically. Their convergence seems to be exponential (i.e. faster than linear on the log-log scale) whereas with w_1 (12) and without window functions the convergence is only polynomial (i.e. linear on the log-log scale).

The complexity of phases 1 and 3 in the Algorithm 1 is $\mathcal{O}\big(N \log_2(N)\big)$ and for phase 2 $\mathcal{O}(N)$. Therefore, the complexity of the whole algorithm is determined by the complexity of the FFT algorithm $\mathcal{O}\big(N \log_2(N)\big)$.

Real order differintegrals of real-valued functions should in general be real-valued as well but numerical calculations may cause small imaginary parts for these solutions. They may be ignored or their amplitudes added to the corresponding real parts. Complex order differintegrals of real-valued functions are in general complex-valued [5,6].

It is good to realise that Matlab functions fft and ifft, for example, have the division by N the other way around, but this has no impact on the algorithm.

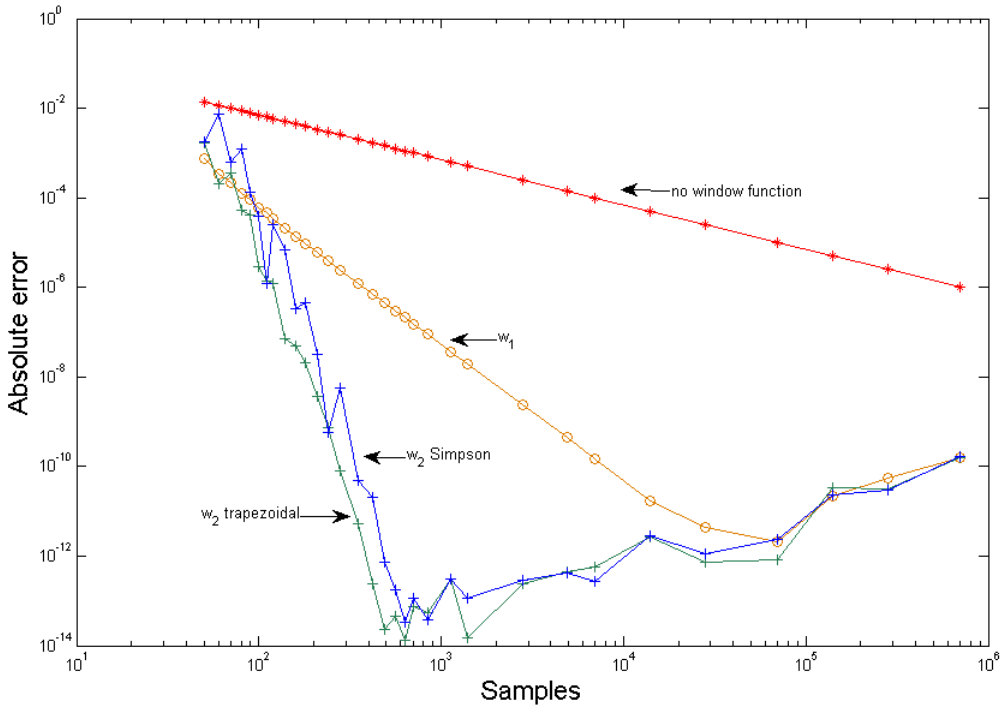

Figure 1. Convergence of the absolute error of the first derivative as the number of sample points increase

3. Generalised norms and MIT indices

3.1 l_p norms and generalised norms

We will focus on differintegrals of order $\alpha \in \mathbb{R}$, although the following norms could also be calculated for $\mathbf{x}^{(z)} \in \mathbb{C}^N$. The differintegrated sequence is represented as a vector

$\mathbf{x}^{(\alpha)} = \left(x_1^{(\alpha)}, x_2^{(\alpha)}, \ldots, x_N^{(\alpha)}\right) \in \mathbb{R}^N$. The l_p *norm* of this sequence is

$$\left\|\mathbf{x}^{(\alpha)}\right\|_p = \left(\sum_{n=1}^{N} \left|x_n^{(\alpha)}\right|^p\right)^{1/p}, \tag{17}$$

where $1 \leq p < \infty$. As p grows, the norms l_p become smaller [16]

$$\left\|\mathbf{x}^{(\alpha)}\right\|_p \geq \left\|\mathbf{x}^{(\alpha)}\right\|_q, \quad \text{if } p < q.$$

Norm l_∞ is the limit as $p \to \infty$ and turns out to be

$$\left\|\mathbf{x}^{(\alpha)}\right\|_\infty = \max_{n=1,\ldots,N} \left|x_n^{(\alpha)}\right|.$$

Norm (17) can be generalised with weight factors, which we choose to be $1/N$ [3,4]. *Generalised norm* $\bar{l}_p$ is $\frac{1}{N}$ *weighted* l_p *norm*

$$\left\|\mathbf{x}^{(\alpha)}\right\|_{p,\frac{1}{N}} = \left(\sum_{n=1}^{N} \frac{1}{N} \left|x_n^{(\alpha)}\right|^p\right)^{1/p} = \left(\frac{1}{N}\right)^{1/p} \left\|\mathbf{x}^{(\alpha)}\right\|_p \tag{18}$$

Norm $\bar{l}_p$ is also called the *power mean* or *Hölder mean* after Otto Hölder and it has the opposite order of growth than l_p norms [17]

$$\left\|\mathbf{x}^{(\alpha)}\right\|_{p,\frac{1}{N}} \leq \left\|\mathbf{x}^{(\alpha)}\right\|_{q,\frac{1}{N}}, \quad \text{if } p < q,$$

but the limit $p \to \infty$ is the same

$$\left\|\mathbf{x}^{(\alpha)}\right\|_{\infty,\frac{1}{N}} = \max_{n=1,\ldots,N} \left|x_n^{(\alpha)}\right|,$$

which is the *peak value*. Norm $p = 2$ is the *root mean square* (rms)

$$\left\|\mathbf{x}^{(\alpha)}\right\|_{2,\frac{1}{N}} = \left(\frac{1}{N}\sum_{n=1}^{N} \left|x_n^{(\alpha)}\right|^2\right)^{1/2}.$$

Peaks and rms values are examples of traditional features calculated from vibration signals.

Clearly there is no reason to limit our attention to so few features, when $\bar{l}_p$ norms can be calculated for any $p \geq 1$. If we do not mind violating the axioms of norms, we can extend these calculations even further. If $p < 1$, the triangle inequality is no longer satisfied and the following features are called quasinorms.

Quasinorm $\bar{l}_0$ is meaningful as a limit $p \to 0$ and turns out to be the *geometric mean*

$$\left\|\mathbf{x}^{(\alpha)}\right\|_{0,\frac{1}{N}} = \left(\prod_{n=1}^{N} \left|x_n^{(\alpha)}\right|\right)^{1/N}.$$

Lahdelma et al. [18] have utilised the cases $0 \leq p < 1$ with good results. With $p < 0$ none of the vector values can be 0. Let us collect these generalisations under one definition,

which is the Hölder mean or generalised norm $\bar{l}_p$. The word 'generalised' then refers not only to weights $1/N$ but also to the inclusion of quasinorms

$$\left\|\mathbf{x}^{(\alpha)}\right\|_{p,\frac{1}{N}} = \begin{cases} \left(\sum_{n=1}^{N} \frac{1}{N} \left|x_n^{(\alpha)}\right|^p\right)^{1/p} & \text{if } p \in \mathbb{R}\backslash\{0\} \\ \left(\prod_{n=1}^{N} \left|x_n^{(\alpha)}\right|\right)^{1/N} & \text{if } p = 0 \\ \max_{n=1,\ldots,N} \left|x_n^{(\alpha)}\right| & \text{if } p = \infty \\ \min_{n=1,\ldots,N} \left|x_n^{(\alpha)}\right| & \text{if } p = -\infty. \end{cases} \tag{19}$$

From the results above we can see that $\bar{l}_p$ norms form a continuous measurement scale for the magnitude of vector signals. Large p values amplify the biggest elements of vectors and small p values the smallest ones. Compare this with differintegrals, where differentiation amplifies high frequencies and integration lower frequencies.

3.2 MIT index

Lahdelma presented in 1992 [19] *the measurement index*, or MIT index, utilising rms values of displacement and its derivatives and integrals of order $n \in \mathbb{N}$. Later it has been generalised to $\bar{l}_p$ norms and real order derivatives and integrals [3,4]. Thus it is formulated as

$${}^{\tau}MIT_{\alpha_1,\alpha_2,\ldots,\alpha_n}^{p_1,p_2,\ldots,p_n} = \frac{1}{n}\sum_{k=1}^{n} b_{\alpha_k} \frac{\left\|\mathbf{x}^{(\alpha_k)}\right\|_{p_k}}{\left(\left\|\mathbf{x}^{(\alpha_k)}\right\|_{p_k}\right)_0}, \tag{20}$$

where $\sum_{k=1}^{n} b_{\alpha_k} = 1$, τ is signal length and the signals with lower index 0 are reference values of the machine in good condition. MIT index can also be combined with other quantities that are related to its condition, such as temperature, pressure or some statistical features of different signals. The weight factors b_{α_k} are used to take into account the severity of different faults occurring at different α_k and p_k. The inverse of MIT index is defined as *condition index* SOL

$$SOL = \frac{1}{MIT}. \tag{21}$$

When the machine is in good condition, the two indices are equal, i.e. $MIT = SOL = 1$. As its condition becomes weaker, growth of the MIT index and decrease of the SOL index usually occur. The word 'usually' is necessary, since, for example, minor wear on new parts may cause smoother operation at the beginning of their usage and hence temporarily reduce MIT.

4. Data acquisition

Four SKF CMPT 2310 accelerometers were mounted externally onto the LHD's front axle housing to measure horizontal and vertical vibrations near the planetary gearboxes on either side. These four vibration measurements together with a tachometer pulse from the drive shaft are recorded with a National Instruments CompactRIO 9024 data logger into a solid-state drive (SSD) as files of one minute length. Signals are recorded with sampling frequency 12800 Hz, and a built-in antialising filter guarantees that there are

no aliases at frequencies that are less than $0.45 \cdot 12800\,\mathrm{Hz} = 5760\,\mathrm{Hz}$. More information on the measurements can be found from an article by Laukka et al. [20].

The measurement points are right vertical (RV), left vertical (LV), right horizontal (RH) and left horizontal (LH). During the first month of the measurements, the accelerometer cables of LV and LH were broken. The accelerometers were replaced and the cables have remained intact since. Two SSDs also broke down after six months of service, which stopped the whole measurement for a month and a half. A third accelerometer at RH broke down during this stoppage and was replaced. At the beginning, measurements were always recorded when the LHD was operating. After the stoppage the program was modified to record only two hours of data after the starting of the LHD.

5. Results

For calculations 106 signals were selected from the beginning of most measurement days, when the rotational frequency of the drive shaft was approximately 13.5 Hz. From each signal a 4 second sample was multiplied with the window function (13) using $\epsilon = 10$ and this new signal was differintegrated with the Algorithm 1. High-pass filtering was performed with an ideal filter at 3 Hz to remove unreliable low-frequency components, and different low-pass filterings at cut-off frequencies 2000 Hz, 3000 Hz and 5000 Hz were also performed with an ideal filter. From each end of the signal 20% was rejected and the remaining 2.4 second signal was used in the calculation of $\bar{l}_p$ norms. All the calculations were performed with Matlab.

Figure 2 shows the 4 s samples from the first and last days of the measurements and their amplitude spectra from the point RV. The vibration level has risen from approximately $12\,\mathrm{m/s^2}$ to $16\,\mathrm{m/s^2}$ and on the first day the two biggest components in the spectrum were approximately at frequencies 1610 Hz and 1880 Hz and on the last day at 1990 Hz and 2540 Hz. Figure 3 shows the corresponding signals from the point LV. Here the vibration level has risen from approximately $12\,\mathrm{m/s^2}$ to $23\,\mathrm{m/s^2}$ and on the first day the two biggest components in the spectrum are approximately at frequencies 1070 Hz and 1500 Hz and on the last day at 1440 Hz and 1670 Hz.

The differential of the front axle has a driving pinion with 9 teeth and a crown wheel with 46 teeth. The planetary gearboxes consist of a stationary ring gear (104 teeth), three planetary gears (39 teeth) and a sun gear (19 teeth). Drive is provided via the sun gear and the planet carrier provides the output to the front wheel. Assuming then that the rotational frequency of the drive shaft is $\nu_{drive} = 13.5\,\mathrm{Hz}$ and that the LHD is not turning, we get the rotational frequency of the sun gear $\nu_{sun} = \frac{9}{46}\nu_{drive}$ and the planetary gear mesh frequency [21,22]

$$\nu_{mesh} = \frac{19 \cdot 104}{19 + 104}\nu_{sun} \approx 42.4\,\mathrm{Hz}.$$

This and its second harmonic $2 * \nu_{mesh}$ can be found from the spectra, but they are insignificant when compared to higher frequency components that dominate the spectra of Figures 2 and 3.

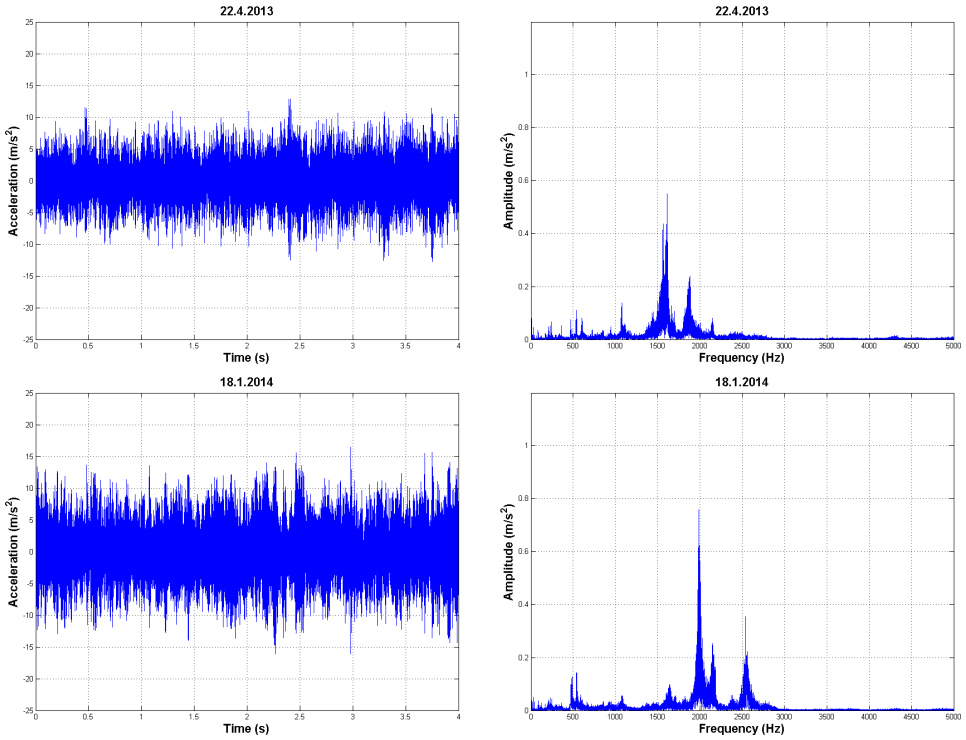

Figure 2. Signals and their amplitude spectra from the point RV at the beginning and end of the measurement period

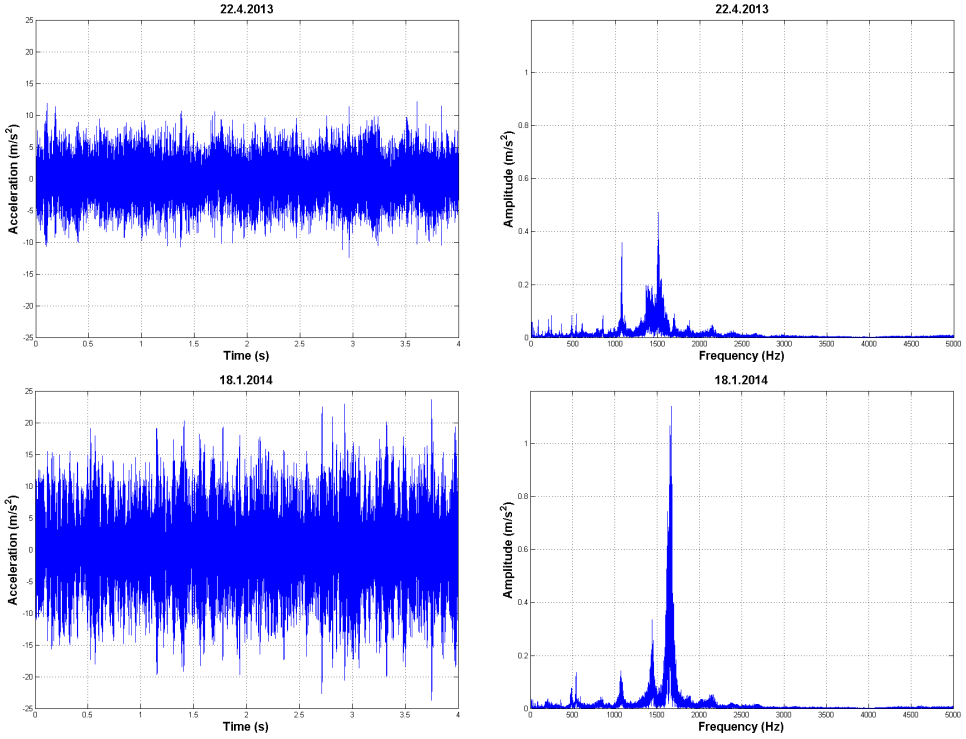

Figure 3. Signals and their amplitude spectra from the point LV at the beginning and end of the measurement period

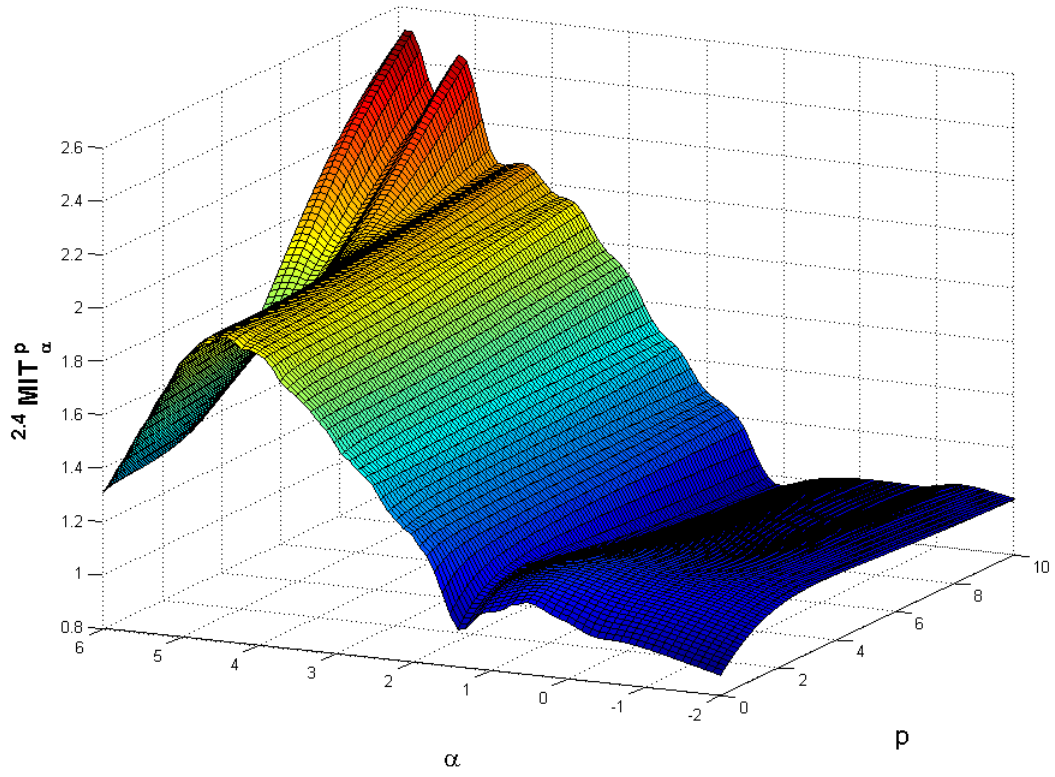

Figure 4. $^{2.4}MIT^{p}_{\alpha}$ surface from the point RV in the frequency range 3 - 5000 Hz

Figure 4 shows a surface that has $^{2.4}MIT^{p}_{\alpha}$ values from the point RV with $0 \leq p \leq 10$ and $-2 \leq \alpha \leq 6$ using a step of 0.1. The values for $^{2.4}MIT^{p}_{\alpha}$ are obtained using the last and first day measurements. The measurements from the first day are used as reference measurements in all the calculations in this paper. Significant changes have taken place. Although these surfaces vary slightly from day to day, the ridge at approximately $\alpha = 4.4$ has constantly been getting bigger with time. The two peaks that occur at the high values of p and α are not the best choices for trend analysis, because the norm values vary too much between days for those values. One also notices that at $\alpha = 2$, which are values of the original acceleration signal, sensitivity is fairly low. This is also seen in the trend analysis of the whole measurement period. Figure 5 shows the trend of right vertical measurements using the values $^{2.4}MIT^{2}_{2}$. The variance in the values is most probably due to the changing terrain and minor fluctuations in the speed of the LHD. The values fall at the beginning but then they bounce around 1 for a long time. Only some time after 200 days the $^{2.4}MIT^{2}_{2}$ values stay above 1.2. The highest value is almost 1.8.

Figure 6 shows another trend of the same signals but this time using the derivative $\mathbf{x}^{(4.4)}$ and $p = 10$. Now the values start to rise very quickly and after 75 days they are always bigger than 1.2. At the end of the measurement period the values almost reach 2.6. This is probably a sign of wear on the gearbox components. The $^{2.4}MIT^{10}_{4.4}$ values increase almost linearly with time.

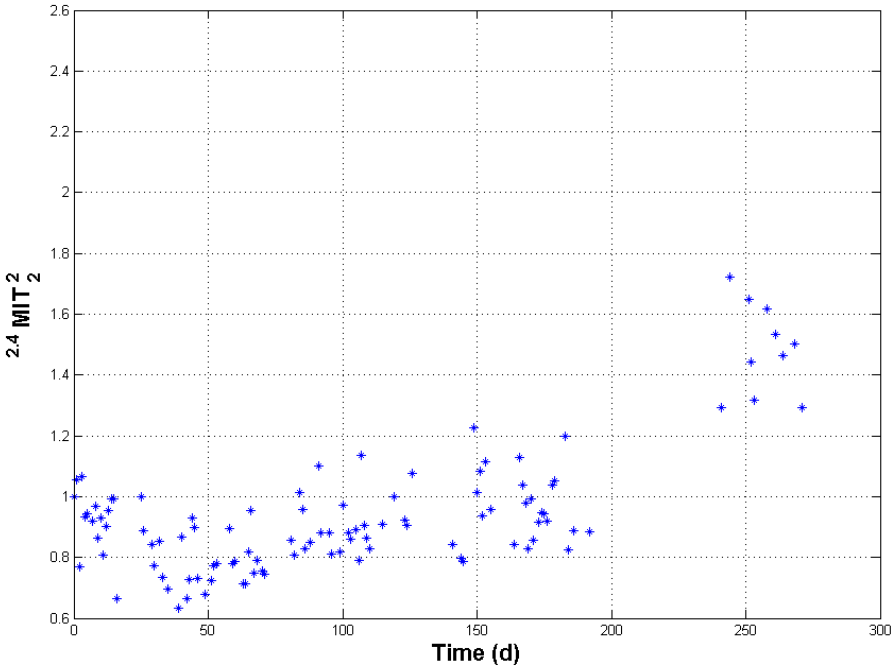

Figure 5. Trend of $^{2.4}MIT_2^2$ from the point RV in the frequency range 3 - 5000 Hz

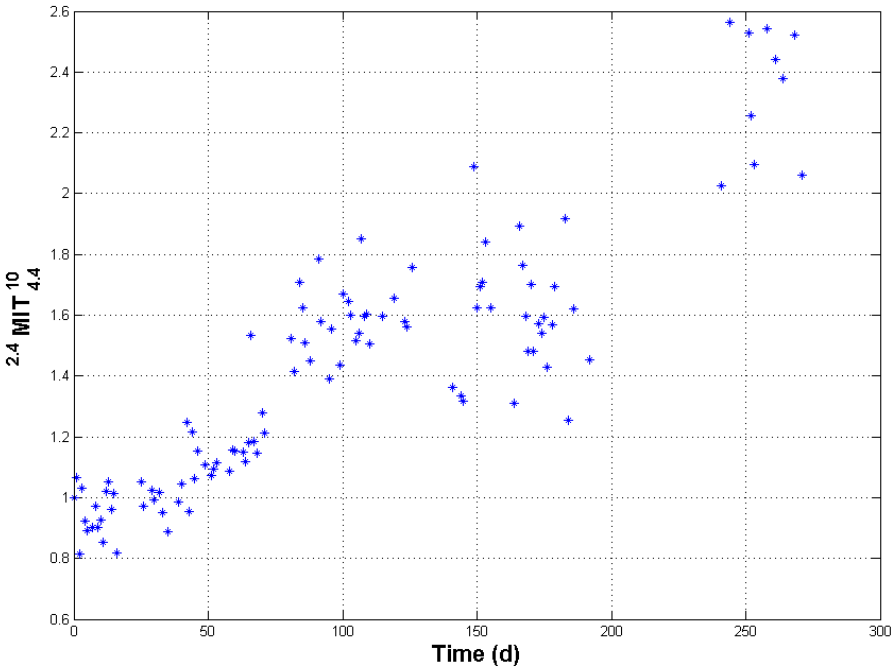

Figure 6. Trend of $^{2.4}MIT_{4.4}^{10}$ from the point RV in the frequency range 3 - 5000 Hz

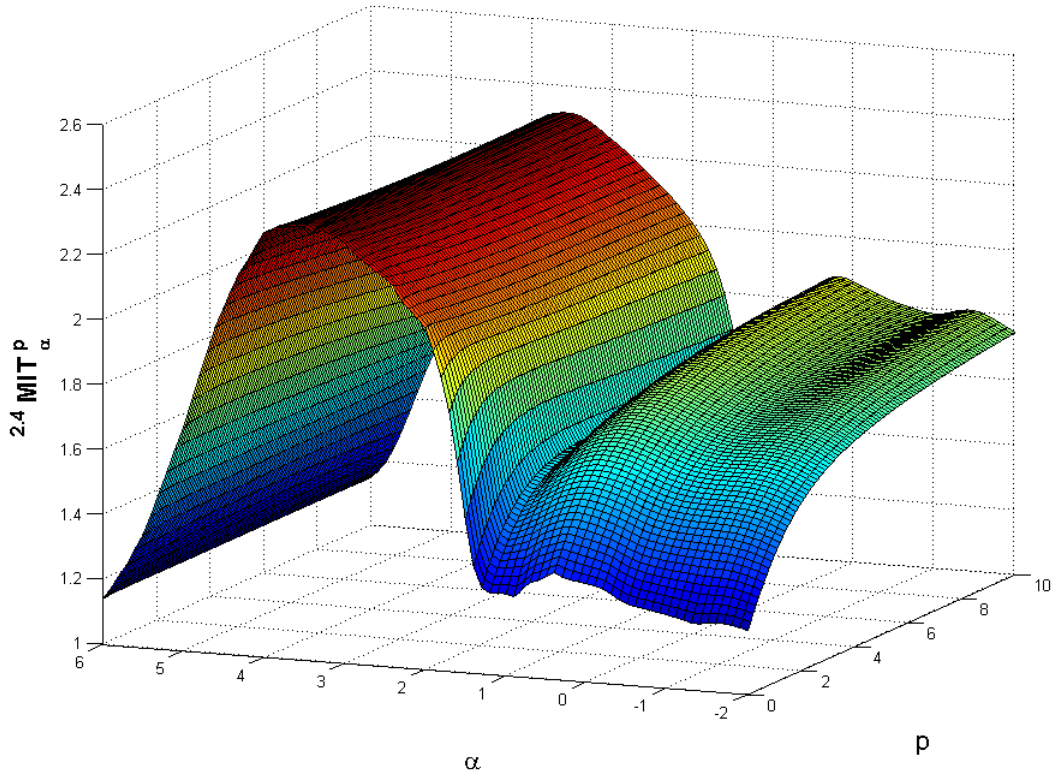

Figure 7. ${}^{2.4}MIT^{p}_{\alpha}$ surface from the point LV in the frequency range 3 - 5000 Hz

Figure 7 shows a surface of ${}^{2.4}MIT^{p}_{\alpha}$ values from the point LV with $0 \leq p \leq 10$ and $-2 \leq \alpha \leq 6$ using a step of 0.1. Its shape differs quite a lot from that of Figure 4, but a similar prominent ridge is present, this time around $\alpha = 3.6$. Integrated values have also risen but they are not suitable for trend analysis because there is too much variation between the measurement days. Figures 8 and 9 show trends from the point LV with rms of the original acceleration signal and $\mathbf{x}^{(3.6)}$ respectively. Using $\alpha = 3.6$ in the trend analysis improves sensitivity in the end, but does not quicken the observation of wear. It looks like the MIT indices rise exponentially with time.

Since the biggest frequency components from the point RV were below 3000 Hz and from the point LV below 2000 Hz, the calculations were repeated in the frequency ranges 3 - 3000 Hz and 3 - 2000 Hz. Figure 10 shows a surface of values ${}^{2.4}MIT^{p}_{\alpha}$ from the point RV with $0 \leq p \leq 10$ and $-2 \leq \alpha \leq 12$ using a step of 0.2 in the frequency range 3 - 3000 Hz and Figure 11 shows the corresponding values calculated from the point LV in the frequency range 3 - 2000 Hz. In both the cases there is a ridge centered at $\alpha = 10$. Since the order of norm seems to have little effect, the trend analysis is performed with easy to calculate $p = 1$ values. The trend of ${}^{2.4}MIT^{1}_{10}$ values for these measurement points are plotted in Figures 12 and 13. The ${}^{2.4}MIT^{1}_{10}$ values from the point RV are doubled after only 50 days and the highest value reached is over 6. For the point LV the highest value reached is over 4, but again the wear is clearly revealed only after 200 days.

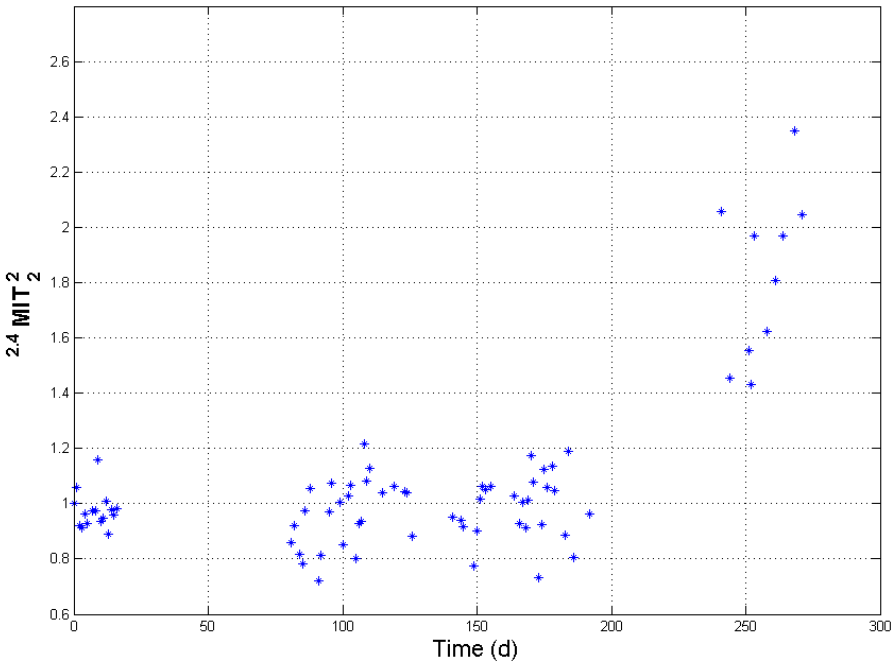

Figure 8. Trend of $^{2.4}MIT_2^2$ from the point LV in the frequency range 3 - 5000 Hz

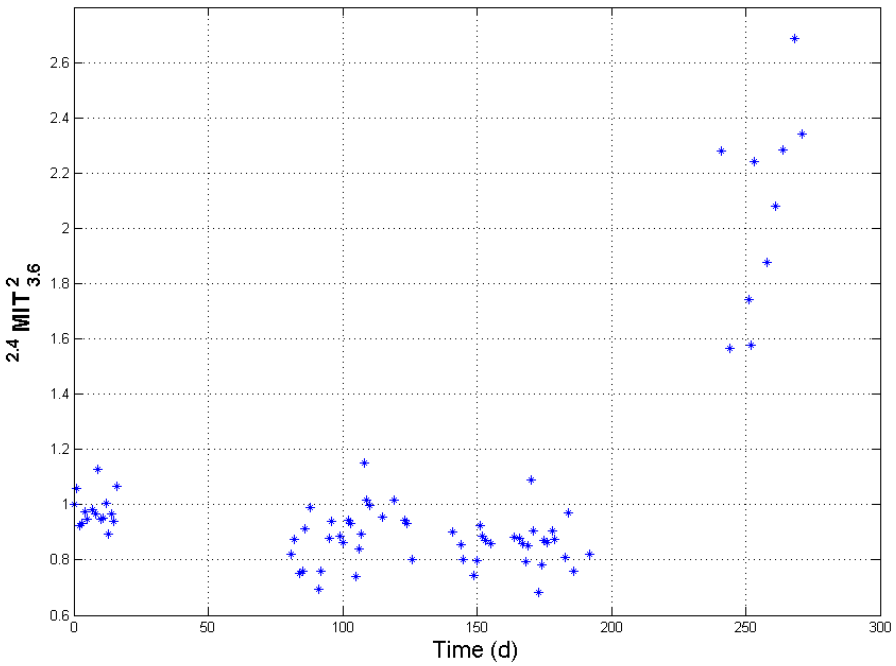

Figure 9. Trend of $^{2.4}MIT_{3.6}^2$ from the point LV in the frequency range 3 - 5000 Hz

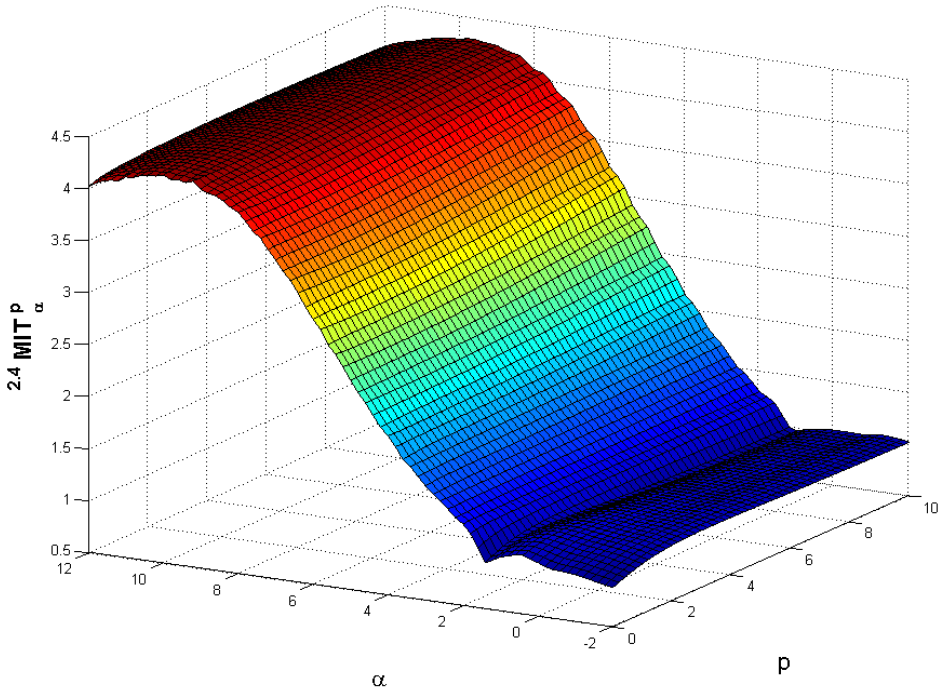

Figure 10. ${}^{2.4}MIT^{p}_{\alpha}$ **surface from the point RV in the frequency range 3 - 3000 Hz**

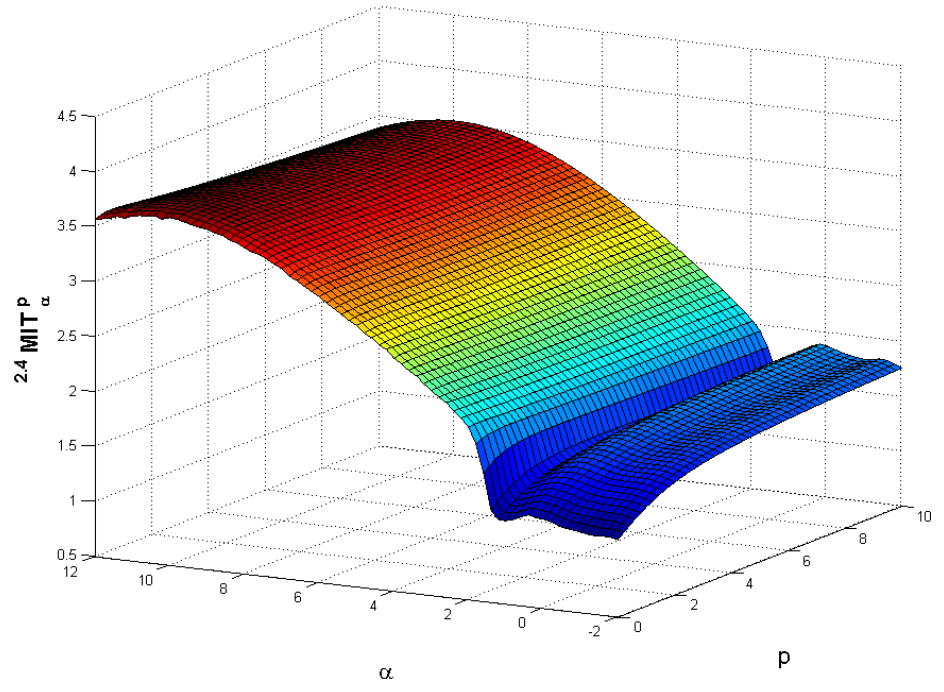

Figure 11. ${}^{2.4}MIT^{p}_{\alpha}$ **surface from the point LV in the frequency range 3 - 2000 Hz**

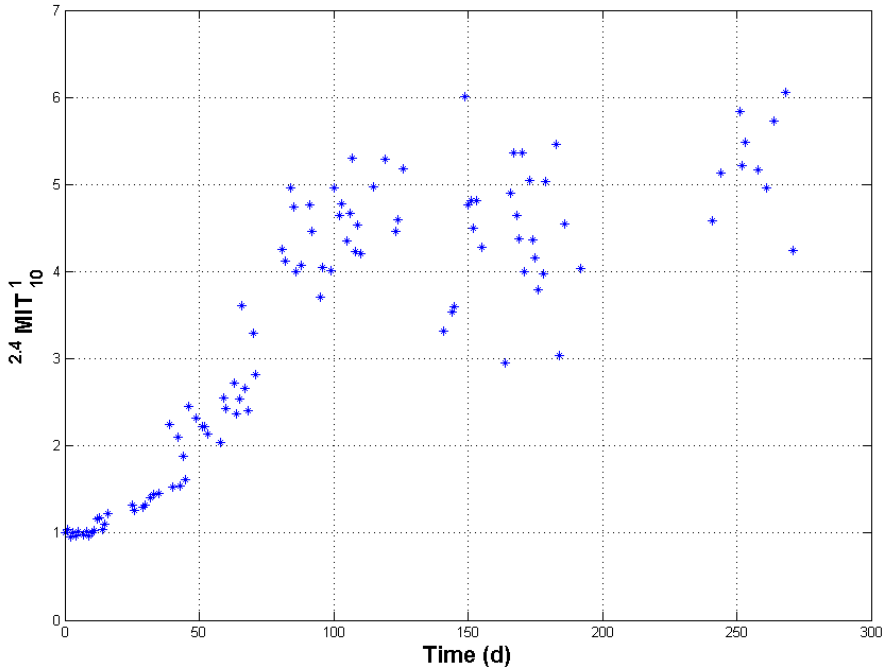

Figure 12. Trend of $^{2.4}MIT_{10}^{1}$ from the point RV in the frequency range 3 - 3000 Hz

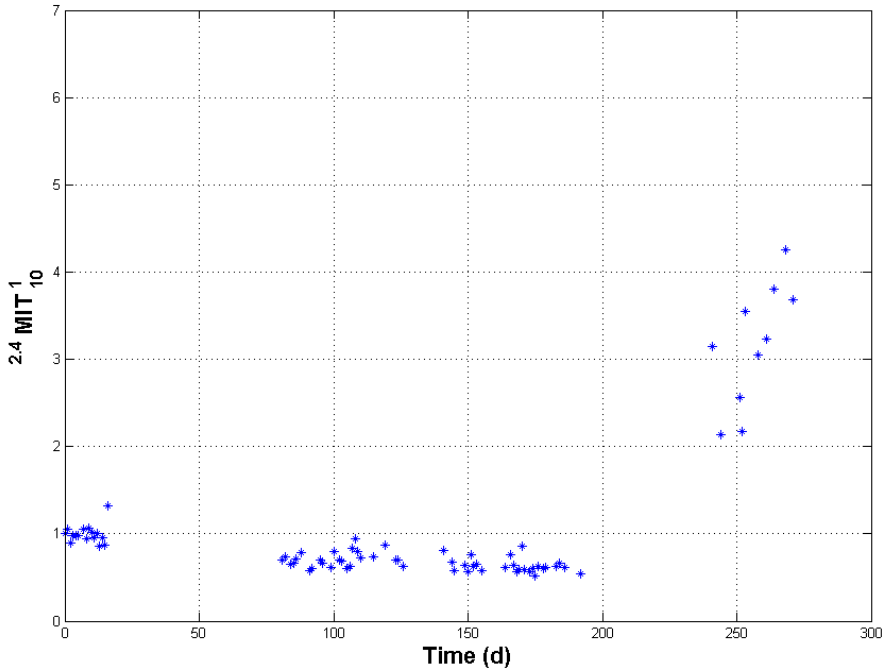

Figure 13. Trend of $^{2.4}MIT_{10}^{1}$ from the point LV in the frequency range 3 - 2000 Hz

Horizontal measurements have not changed as much. This can be seen from the trends of the rms values of horizontal acceleration signals in Figures 14 and 15. Values ${}^{2.4}MIT_2^2$ from the point RH seem to have risen at the beginning, but they return back to around 1 at the end of the measurement period. No clear trend is imminent and ${}^{2.4}MIT_\alpha^p$ surfaces also vary considerably from day to day.

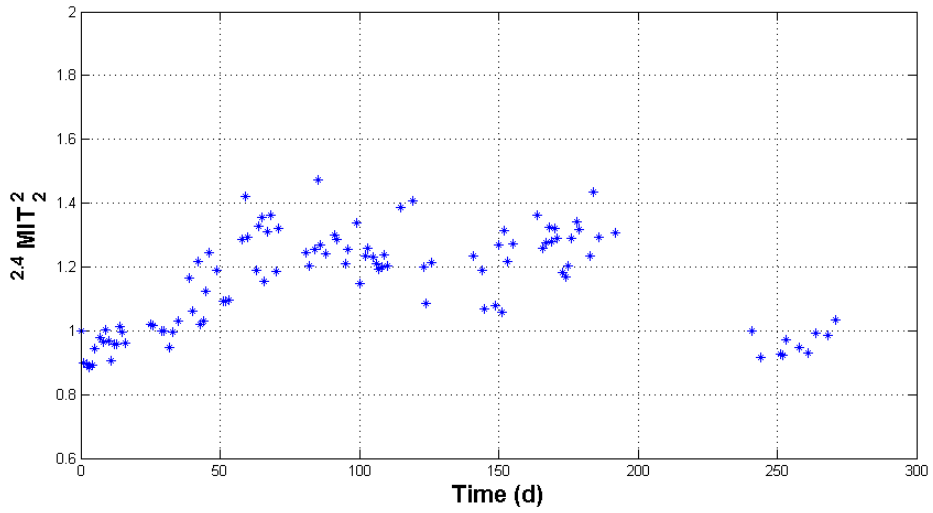

Figure 14. Trend of ${}^{2.4}MIT_2^2$ from the point RH in the frequency range 3 - 5000 Hz

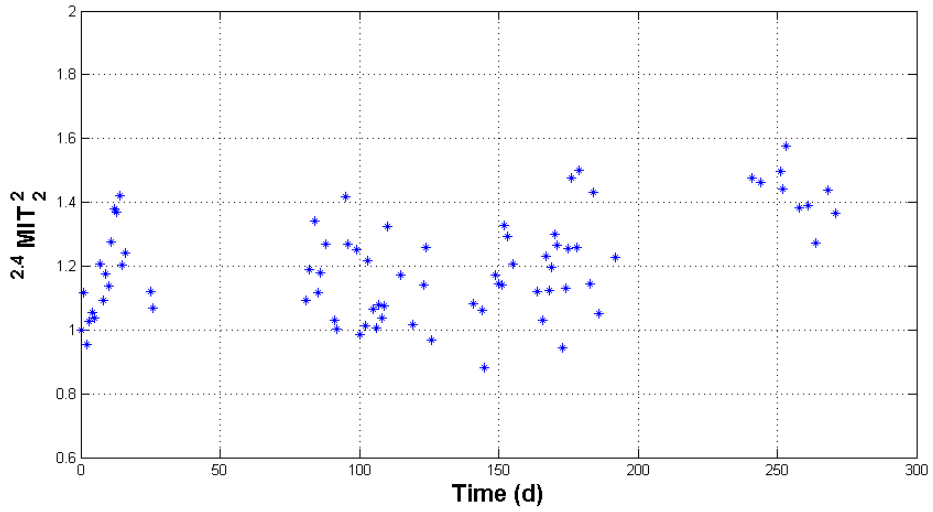

Figure 15. Trend of ${}^{2.4}MIT_2^2$ from the point LH in the frequency range 3 - 5000 Hz

6. Conclusions

Real order derivatives and integrals are simple and fast to calculate in the frequency domain. Together with Algorithm 1 and window function (13), the results are also very reliable, although the significance of this window function and the multiplier for the $N/2$ term in the Algorithm 1 becomes less important when N is big. Combined with generalised norms, one can plot a surface using the values of the MIT index. This surface is suitable for searching the optimal values for α and p in fault detection.

It is difficult to monitor the condition of a mobile vehicle. In this case the LHD is fortunately operated without load at almost constant speed nearly every morning. Vertical vibrations measured during constant speed and in the case of no load increased during the 271 days. The differentiation of the signals improves sensitivity. The order of norm only seems to have little effect in this study. In the frequency range 3 - 3000 Hz the ${}^{2.4}MIT_{10}^{1}$ index from the point RV has doubled only after 50 days and the highest value reached is over 6. In the frequency range 3 - 2000 Hz, the ${}^{2.4}MIT_{10}^{1}$ index from the point LV has exceeded 4, but has changed significantly only after 200 days. This probably means that the gearbox components on right side have constantly suffered wear during the whole measurement period but on the left side they have suffered considerable wear only recently.

Measurements are still running and the damage in the axle has not yet been inspected. To utilise signals from the working stages of the LHD, measurements should incorporate more data from the LHD, especially its load. Otherwise the signals are hardly comparable.

References

1. S Lahdelma, 'On the Derivative of Real Number Order and its Application to Condition Monitoring', Kunnossapito, Vol 11, No 4, pp 25-28, 1997.

2. S Lahdelma and V Kotila, 'Real order derivatives - New signal processing method', in Finnish, Kunnossapito, Vol 17, No 8, pp 39-42, 2003.

3. S Lahdelma and E Juuso, 'Signal processing and feature extraction by using real order derivatives and generalised norms. Part 1: Methodology', The International Journal of Condition Monitoring, Vol 1, No 2, pp 46-53, 2011.

4. S Lahdelma and J Laurila, 'Detecting misalignment of a claw clutch using vibration measurements', In Proceedings of CM2012/MFPT 2012, The Ninth International Conference on Condition Monitoring and Machinery Failure Prevention Technologies, London, UK, 12^{th} - 14^{th} June 2012.

5. S Lahdelma, 'On the Derivative of Complex Number Order and its Application to Condition Monitoring and Active Control', Kunnossapito, Vol 13, No 1, pp 27-34, 1999.

6. S Lahdelma and V Kotila, 'Complex Derivative - A New Signal Processing Method', Kunnossapito, Vol 19, No 4, pp 39-46, 2005.

7. J Fourier, 'Théorie analytique de la chaleur', Firmin Didot, Paris, 1822.

8. P Závada, 'Operator of fractional derivative in the complex plane', Communications in Mathematical Physics, Vol 192, No 2, pp 261-285, 1998.

9. R Herrmann, 'Fractional Calculus: An Introduction For Physicists', World Scientific Publishing Company, 2011.

10. H Weyl, 'Bemerkungen zum Begriff des Differentialquotienten gebrochener Ordnung', Vierteljahrsschrift der Naturforschenden Gesellschaft in Zürich, Vol 62, No 1-2, pp 296-302, 1917.

11. S G Samko, A A Kilbas and O I Marichev, 'Fractional Integrals and Derivatives. Theory and Applications', Gordon and Breach, Amsterdam, 1993.

12. R W Hamming, 'Digital filters', Prentice-Hall, Englewood Cliffs, New Jersey, 1977.

13. D E Newland, 'An Introduction to Random Vibrations, Spectral & Wavelet Analysis', 3rd ed. Longman Scientific & Technical, Essex, 1993.

14. S G Johnson, 'Notes on FFT-based differentiation' `http://math.mit.edu/~stevenj/fft-deriv.pdf`, 2011. Retrieved 11.4.2014.

15. J W Cooley and J W Tukey, 'An Algorithm for the Machine Calculation of Complex Fourier Series', Mathematics of Computation, Vol 19, No 90, pp 297-301, 1965. `http://www.jstor.org/stable/2003354?seq=1`. Retrieved 11.4.2014.

16. E M Stein and R Shakarchi, 'Princeton Lectures in Analysis IV Functional Analysis: Introduction to Further Topics in Analysis', Princeton University Press, Princeton, New Jersey, 2011.

17. P S Bullen, 'Handbook of Means and Their Inequalities', 2nd ed. Kluwer Academic Publishers, Dordrecht, 2003.

18. J Laurila and S Lahdelma, 'Condition monitoring by means of vibration and sound measurements', In Proceedings of CM2013/MFPT 2013, The Tenth International Conference on Condition Monitoring and Machinery Failure Prevention Technologies, Kraków, Poland, 18^{th} - 20^{th} June 2013.

19. S Lahdelma, 'New vibration severity evaluation criteria for condition monitoring', in Finnish, University of Oulu, Research report No 85, 1992.

20. A Laukka, J Saari, J Ruuska, E Juuso and S Lahdelma, 'Condition based monitoring for underground mobile machines', In Proceedings of MPMM 2013, Lappeenranta, Finland, 12^{th} - 13^{th} September 2013.

21. J Immonen, S Lahdelma and E Juuso, 'Condition monitoring of an epicyclic gearbox at a water power station', In Proceedings of SIMS2012, The 53rd Scandinavian Conference on Simulation and Modelling, Reykjavik, Iceland, 4^{th} - 6^{th} October 2012.

22. C M Vicuña, 'Contributions to the analysis of vibrations and acoustic emissions for the condition monitoring of epicyclic gearboxes', Aachener Schriften zur Rohstoff- und Entsorgungstechnik des Instituts für Maschinentechnik der Rohstoffindustrie, Verlag R. Zillekens, Aachen, 2010.